Preprint Cambridge Centre for Computational Chemical Engineering ISSN 1473 – 4273

Can soot particles burn from the inside?

Peter Grančič [1], Jacob W. Martin [1], Dongping Chen [2], Sebastian Mosbach [1], Markus Kraft [1,3]

released: 20 April 2016

[1] Department of Chemical Engineering and Biotechnology
University of Cambridge
New Museums Site
Pembroke Street
Cambridge, CB2 3RA
United Kingdom
E-mail: mk306@cam.ac.uk

[2] Department of Mechanical Engineering
Stanford University
Building 520
452 Escondio Mall
Stanford, California 94305-3030
United States
E-mail: dc516@stanford.edu

[3] School of Chemical and Biomedical Engineering
Nanyang Technological University
62 Nanyang Drive
6357459
Singapore

Preprint No. 167

UNIVERSITY OF CAMBRIDGE

Keywords: coronene cluster, molecular dynamics, polyaromatic hydrocarbons, specular and diffuse molecular scattering, residence time, interatomic potentials and forces

Edited by
Computational Modelling Group
Department of Chemical Engineering and Biotechnology
University of Cambridge
New Museums Site
Pembroke Street
Cambridge CB2 3RA
United Kingdom

Fax: + 44 (0)1223 334796
E-Mail: c4e@cam.ac.uk
World Wide Web: http://como.cheng.cam.ac.uk/

Abstract

The trajectories of a single nitrogen molecule resulting from a series of collisions with coronene molecular clusters of varying size are determined numerically by means of classical molecular dynamics simulations at two system temperatures, corresponding to the clusters being in solid and liquid state. The observed bimodality of the residence time distributions that corresponds to a combination of specular and diffuse molecular scattering tends to disappear with increasing temperature due to the more rapid rearrangements of the coronene cluster constituent molecules in the liquid state. The mean residence time decreases with increasing system temperature and appears to be independent of the coronene cluster size within the cluster size-range considered here. The recorded trajectories of the nitrogen probe are relatively tortuous, on average one order of magnitude longer than the shortest path connecting the impact and desorption points. The vast majority of the sites visited during the nitrogen molecule residence period correspond to the atoms at the edge of coronene molecules, mainly hydrogens. The intermolecular cohesive forces between the molecules cause that the coronene clusters are impenetrable by the nitrogen probe at temperatures below their thermal dissociation point.

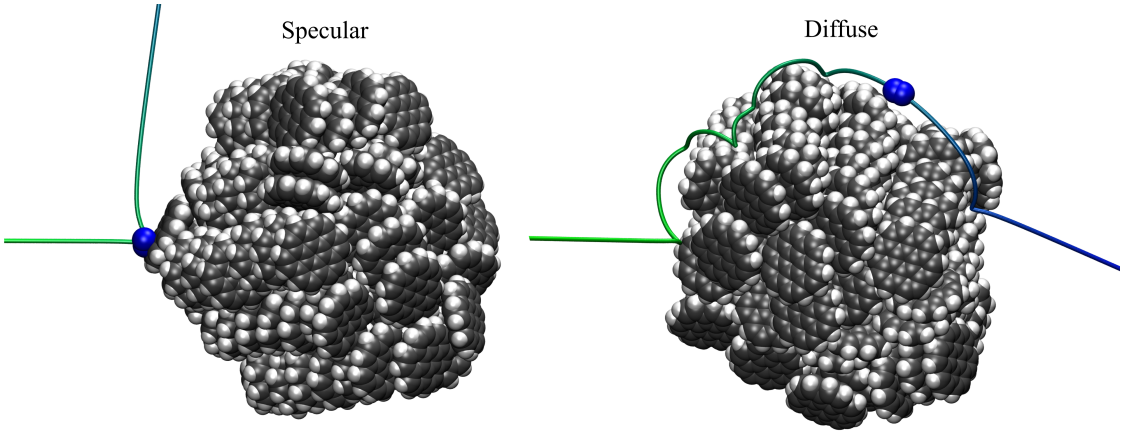

Highlights:

- Collisions between nitrogen molecule and coronene clusters are investigated via classical molecular dynamics simulation.
- Residence time distributions of the nitrogen probe exhibit bimodality, corresponding to a combination of specular and diffuse molecular scattering regimes.
- Nitrogen trajectories are found to be highly tortuous with the majority of atomic sites visited belonging to the edge of the coronene molecules.
- Coronene clusters are shown to be impenetrable below their thermal dissociation point.

1 Introduction

The formation of solids in flames during combustion has gained a significant amount of attention during the past decades. Not only because carbonaceous soot particles are considered harmful to the environment and human health [28] but also because combustion processes are ever more frequently explored as potential pathways for manufacturing novel materials [2, 34, 40].

Numerous experimental evidence suggests that polyaromatic hydrocarbon (PAH) stacks are the main building blocks of carbonaceous soot particles [1, 14, 15, 29]. PAHs represent the most stable bonding configurations at flame temperatures [39] and their cohesive properties can lead to enhanced stability of PAH stacks if the individual constituent molecules contain at least 10-20 aromatic rings [4, 5].

The growth of soot particles is comprised of two simultaneous processes, chemical growth and particle coagulation [25, 35]. While the latter occurs either via coalescence or aggregation, depending on the size and temperature of the colliding particles [8, 9], the former involves aromatic growth via the hydrogen-abstraction-acetylene-addition (HACA) mechanism [18] and can be counterbalanced by oxidation involving chemical species such as oxygen or hydroxyl radicals [7, 13, 17, 38].

Although the flame environment usually offers sufficient activation energy to trigger chemical reactions, it is equally important that the reactants appear in close proximity for the required amount of time for a chemical reaction to take place. Despite the fact that flames can be characterised as environments with low density and relatively low frequency of collisions, the experimentally observable formation of nanoparticles in flames confirms that processes such as aggregation and growth with or without covalent bonding are possible [47].

There are many gaps in our understanding of growth and the structure of nascent soot particles due to the difficulties in accessing the early stages of their formation experimentally. Therefore, molecular simulations have become a routine tool used in the investigation of many soot-formation related phenomena, such as the determination of stability and favourable geometries of PAH stacks [33], dynamics of PAH dimerisation [36], soot particle inception and aggregation [43, 46] and structure and phase behaviour of nascent soot particles [8, 9, 11, 41].

Surface reactions are subject to many experimental and theoretical investigations and detailed kinetic models for gas-phase reactions, formation, growth and oxidation of soot particles were proposed [30, 35, 37]. One of the open questions remains the accessibility of reactive sites of PAH clusters by small gaseous species at elevated temperatures, particularly sites localised in their interior. This problem was partially addressed previously by applying a static probe to integrate the available surface area for potential chemical reactions using the concept of solvent-excluded surface [10]. However, it is important to note that any surface roughening feature, i.e., a structural feature that increases the particle surface area (such as convex cups, concave pits or saddle belts) has a limited lifetime in dynamic systems at elevated temperatures and in order to predict the accessibility of reactive sites the system dynamics and particularly the kinetic energy transfer resulting from the collisions with potential gaseous reactants has to be taken into account.

The purpose of the present article is to track and analyse the trajectories of two colliding bodies, single nitrogen probe and coronene molecular cluster, as a function of temperature and coronene cluster size by means of classical molecular dynamics (MD) simulations. The choice of nitrogen molecule is supported by its size [3] and mass similarity to the typical soot growth precursors and inhibitors (i.e., acetylene and oxygen molecules, respectively) and its reduced chemical reactivity at elevated temperatures makes it an ideal model system for classical MD simulations. On the other hand, the molecular clusters composed of coronene molecules are often used as the representations of nascent soot particles [8, 41]. By exploring the collision paths, residence time and the sites visited we construct a dynamic model of the gas-soot particle interactions with the aim to answer the question whether gas molecules can enter the interior of soot particles.

2 Simulation methodology

All MD calculations were carried out by using the software GROMACS [44] and a set of home-made scripts to generate the input files, process and visualize the output. The intermolecular interactions are described by combining the isoPAHAP force field [8, 43] accompanied by transferable point charges [42] for C-C, C-H and H-H non-bonded interactions with the Williams 99 force field [48, 49] for C-N and H-N non-bonded interactions, respectively. Following the approach of Coasne et al. [12], the quadrupole moment of the nitrogen molecule is not explicitly given. Instead of using a united-atom approach, the nitrogen molecule is considered to be a harmonic oscillator with the vibrational frequency of $2359\,\mathrm{cm}^{-1}$, leading to the force constant of $1382813.1\,\mathrm{kJ\,mol}^{-1}\,\mathrm{nm}^{-2}$ [24]. The equilibrium N-N bond length is taken from experiments as $0.1098\,\mathrm{nm}$ [20]. The intramolecular terms describing the bonds, angles and dihedrals of the coronene molecules are taken from the OPLS-AA force field [21]. The complete list of force field parameters is listed in Appendix A.

The initial atomic positions and velocities of a set of coronene clusters with varying number of constituent molecules were obtained after a sequence of geometry optimisation, simulated annealing and molecular dynamics equilibration within the NVT ensemble at given temperatures [8] assuring the complete removal of any systematic energy drift in the system.

To sample the collision events, each pre-equilibrated coronene cluster is rotated by a set of three Euler angles drawn randomly from an uniform distribution in the interval of $[-\pi,\pi]$. Next, the nitrogen molecule is positioned outside the interaction cut-off range ($r_{\mathrm{cut}} = 3\,\mathrm{nm}$) and the velocities of the constituent atoms of both objects are modified by adding mutually opposing velocity vectors (considering so-called zero impact factor, i.e., a center-of-mass to center-of-mass collision) of the magnitude corresponding to the root-mean-square velocity, $v_{\mathrm{RMS},i}$, as defined by the Maxwell-Boltzmann distribution at given temperature, T, $v_{\mathrm{RMS},i} = \sqrt{3k_{\mathrm{B}}T/m_i}$, with k_{B} and m_i denoting the Boltzmann constant and mass of ith particle, respectively. Typical values of the root-mean-square velocity of the nitrogen molecule are $0.5968\,\mathrm{nm\,ps}^{-1}$ and $0.7309\,\mathrm{nm\,ps}^{-1}$ for $T = 400\,\mathrm{K}$ and $T = 600\,\mathrm{K}$, respectively. For each temperature and coronene cluster size, a series of at least 1000 simulations were performed to obtain reasonable statistics.

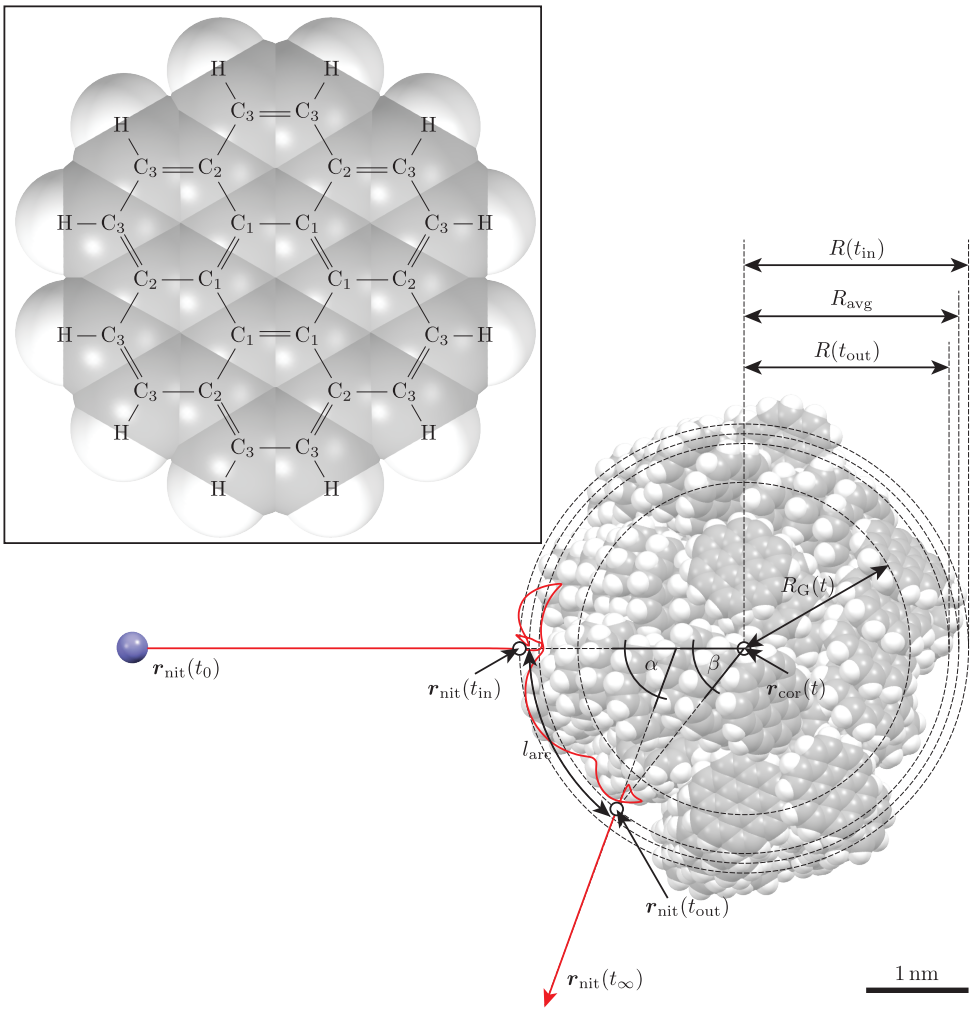

Figure 1: *Geometry of collision events. The bold red line denotes the trajectory of the center-of-mass of the nitrogen molecule,* $\boldsymbol{r}_{\mathrm{nit}}(t)$*. The position of the center-of-mass of the coronene cluster and its radius of gyration are denoted by the symbols* $\boldsymbol{r}_{\mathrm{cor}}(t)$ *and* $R_{\mathrm{G}}(t)$*, respectively. The residence time,* t_{res}*, the actual path length,* l*, and the arc length,* l_{arc}*, are confined by the points* $\boldsymbol{r}_{\mathrm{nit}}(t_{\mathrm{in}})$ *and* $\boldsymbol{r}_{\mathrm{nit}}(t_{\mathrm{out}})$*. Both* t_{in} *and* t_{out} *are defined as the first and last moments in time when the nearest distance between the center-of-mass of the nitrogen molecule and any constituent atom of the coronene cluster is less than a given threshold, here* 0.346 nm *(defined as the distance corresponding to the H-N potential energy minimum). The symbols* α *and* β *denote the scattering and absorption-trapping-desorption angles. The arc length* l_{arc} *is based on averaging the distances between impact and desorption points to the coronene cluster center-of-mass,* $R_{\mathrm{avg}} = [R(t_{\mathrm{in}}) + R(t_{\mathrm{out}})]/2$*. The inset displays the coronene molecule composed of four types of atoms, i.e,* C_1*,* C_2*,* C_3 *and* H*, respectively.*

The actual MD simulations of the collisions were performed within the NVE ensemble, conserving the total energy of the system and the Newtonian equations of motion were in-

tegrated with the velocity-Verlet integration scheme [45]. For each simulation, the atomic trajectories were recorded for a time frame of 40 ps with the time step of 10 fs to cover the entire collision event with sufficient resolution.

The spatio-temporal evolution of the collision event is monitored using the following measures (cf. Figure 1): (i) the residence time, t_{res}, i.e., the time the nitrogen molecule spends trapped at the surface of the coronene cluster, (ii) the scattering angle, α, i.e., the angle between the initial and terminal trajectories of the nitrogen molecule, expressed as the angle between velocity vectors prior to impact with the cluster and after the molecule has detached from the cluster, respectively, (iii) the absorption-trapping-desorption angle, β, i.e., the central angle between the points of initial impact and final detachment, where the term "central" refers to the centre-of-mass of the cluster, (iv) the actual path length, l, i.e., the total path length taken by the nitrogen molecule during the residence period, (v) the arc length, l_{arc}, i.e., the length of an arc connecting the impact and detachment points drawn on the surface of a sphere of radius given by their average distance to the center-of-mass of the cluster, and (vi) the tortuosity of the path taken, τ, defined as the ratio between the actual and arc path lengths, $\tau = l/l_{\mathrm{arc}}$. During the residence period, (vii) the center-of-mass distance between both objects is recorded and normalised by the gyration radius of the coronene cluster, R_{G}, with the dimensionless minimum value denoted as d_{min}. Finally, (viii) the identity (cf. Figure 1, inset) of coronene atomic sites visited by the nitrogen probe during the residence period is determined. This is based on the shortest Euclidean distance between the center-of-mass of the nitrogen probe and the position of a given atom by taking its Van der Waals radius into account. The Van der Waals radii considered here are 0.12 nm for hydrogen and 0.17 nm for carbon atoms, respectively [3]. However, only time steps during which the nitrogen probe remains in close proximity of the coronene cluster (defined by a 0.346 nm cut-off) are taken into account and expressed as the cummulative frequency for a given collision event, $\sum_i w_i$ (with i denoting C_1, C_2, C_3 or H atom sites; cf. Figure 1, inset).

3 Results and discussion

In order to sample the morphology and dynamics of the coronene clusters, three different coronene cluster sizes (composed of 50, 100 and 200 molecules, having the average radii of 1.7, 2.3 and 2.8 nm, respectively) at two temperatures ($T = 400$ and 600 K) were considered. It is well known that the melting points of nano-clusters strongly depend on their size [6, 9, 26, 27]. The melting points of the coronene clusters considered in this work were determined previously as 455, 500 and 525 K for clusters consisting of 50, 100 and 200 coronene molecules, respectively, by averaging the values of two parameters reflecting the mobility and thermally-driven disorder of the constituent molecules, the intermolecular energy and Lindemann index obtained from MD simulations over a relatively wide range of temperatures [8]. Hence, in this work we have chosen two environmental temperatures that correspond to the clusters being in solid ($T = 400$ K) and liquid ($T = 600$ K) state.

Figure 2 shows the residence time distributions as recorded for the three different coronene cluster sizes at two environmental temperatures. The range of values for the recorded res-

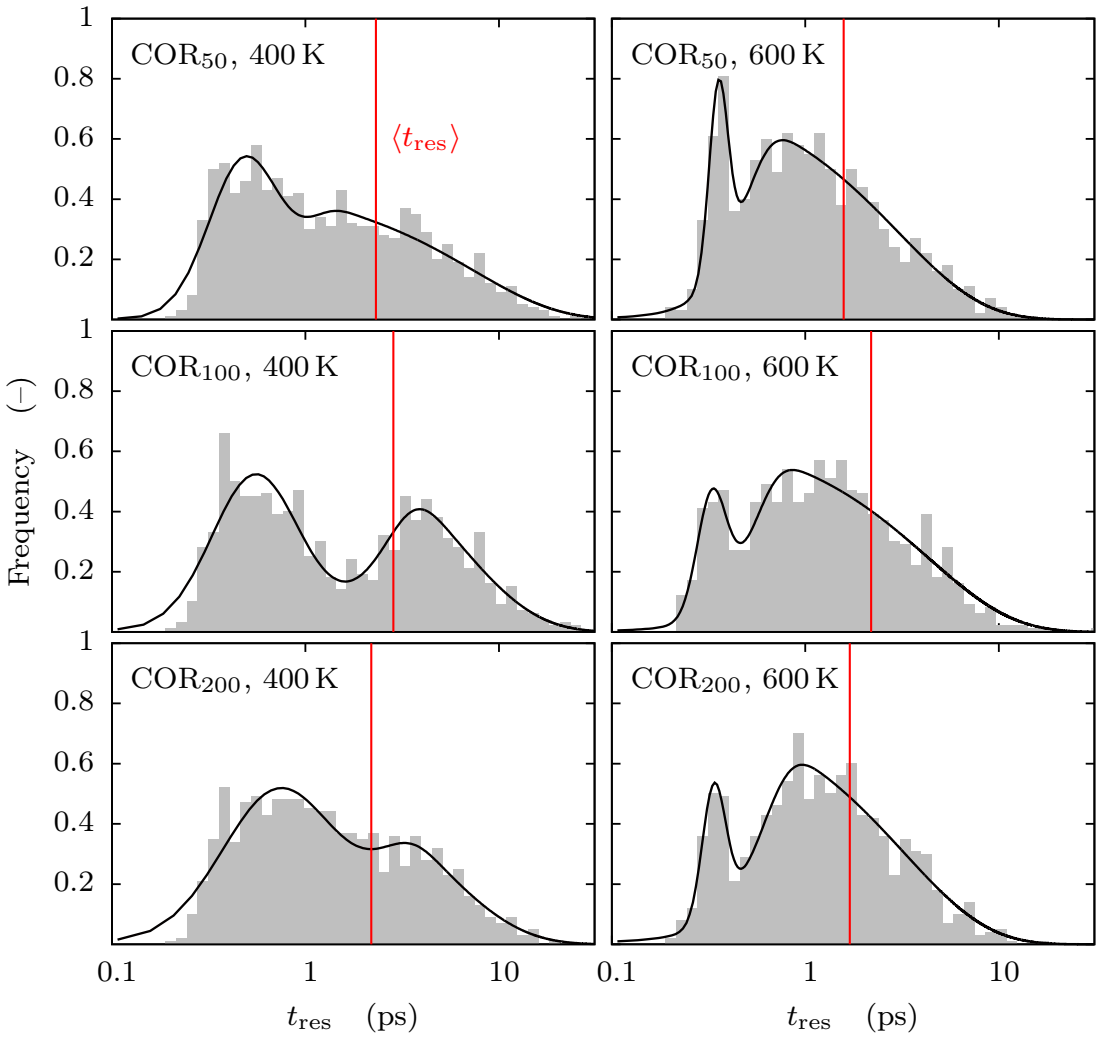

Figure 2: *Residence time distributions. Collision events that result in relatively short residence times ($t_{res} < 1$ ps) are the outcome of immediate reflection, corresponding to the specular scattering regime. On the other hand, collision events with longer residence times are considered to be the result of diffuse scattering regime. The solid red lines denote the mean residence time, $\langle t_{res} \rangle$.*

idence times, t_{res}, is rather wide and its bimodality suggests the presence of both types of known molecular scattering regimes, i.e., an immediate specular and a longer diffuse molecular scattering regime. The diffuse scattering regime represents an intermediate between permanent absorption and immediate reflection which occurs when the particle size becomes significantly larger compared to the gaseous species (usually several nanometers in radius, $R \approx 2.5$ nm) and the gas molecule is able to perform hops along the particles' surface [22, 23].

The drastic rearrangements of the constituent molecules associated with higher thermal

velocities in the liquid state ($T = 600\,\mathrm{K}$) lead to rapidly changing nitrogen-coronene interactions, switching them from attractive to repulsive and *vice-versa*. Consequently, collision events that result into residence times around 1 ps become more populated and the mean residence time, $\langle t_{\mathrm{res}} \rangle$, decreases (cf. the red lines in Figure 2).

It is generally accepted that the gas-particle attraction increases with the size of the particles [23]. However, the coronene cluster size range considered here is either too narrow to have any significant effect on the mean residence time and/or the stacked conformational coronene building components and their overall dynamics affect the collision event in a similar manner regardless the actual size of the coronene cluster. There are two factors that determine the collision regime at the molecular level, (i) the strength and (ii) the shape of the field between the nitrogen molecule and the coronene cluster. While the strength of the field is primarily associated with the size and density of the coronene clusters, its shape is a function of the local molecular arrangements (often referred to as the surface roughness) at the impact zone. Both factors remain roughly constant for a given temperature causing negligible difference in the recorded mean residence time values for the varying coronene cluster size.

We have extensively investigated the structural features of the impact zones of the coronene clusters by a variety of methods (e.g., by determining the local orientation of the nearest coronene molecules, the presence and size of a cavity in the impact zone and the identity of the nearest atom at impact) with the aim to identify the factors that may influence the resulting residence time, however, no clear correlation between the observed residence times and any of the selected impact area "order parameter" was found (not shown here).

Figure 3 reveals that the length of the residence trajectory of the nitrogen molecule is approximately 14-fold of that of the shortest distance between the impact and desorption points (as expressed by the value of its average tortuosity factor, $\langle \tau \rangle$). Further, all plots regardless of the simulation set-up have very similar appearance suggesting that the residence paths retain their properties within the given cluster size range and temperatures. The observed tortuosity values can be understood as a measure of the surface roughness (here defined by the strong anisotropy of the constituent coronene molecules) as well as the consequence of the nitrogen molecule being absorbed at the surface and then moving from one potential energy well into another in a random fashion with the possibility of visiting the same potential energy wells repeatedly, depending on their lifetime.

The dependence of both the scattering and the absorption-trapping-desorption angles (α and β, respectively) on the residence time shows that the majority of the surface trajectories terminate before the nitrogen reaches the opposite side of the coronene cluster (cf. Figures 4 and 5). This is no surprise when considering the recorded average tortuosity of the actual paths taken by the nitrogen molecule. As one would further expect, the variance in the absorption-trapping-desorption angle increases with increasing residence time. On the other hand, no correlation can be found between the residence time and the recorded scattering angle distributions as the direction of the terminal trajectory depends strongly on the local arrangement and dynamics of the coronene molecules in the desorption area. Table 1 shows that the average value of the absorption-trapping-desorption angle has a decreasing tendency with increasing coronene cluster size which is in good agreement with previously published results [23]. However, the values of the average absorption-trapping-desorption angles are far from idealised full-sphere diffuse scattering

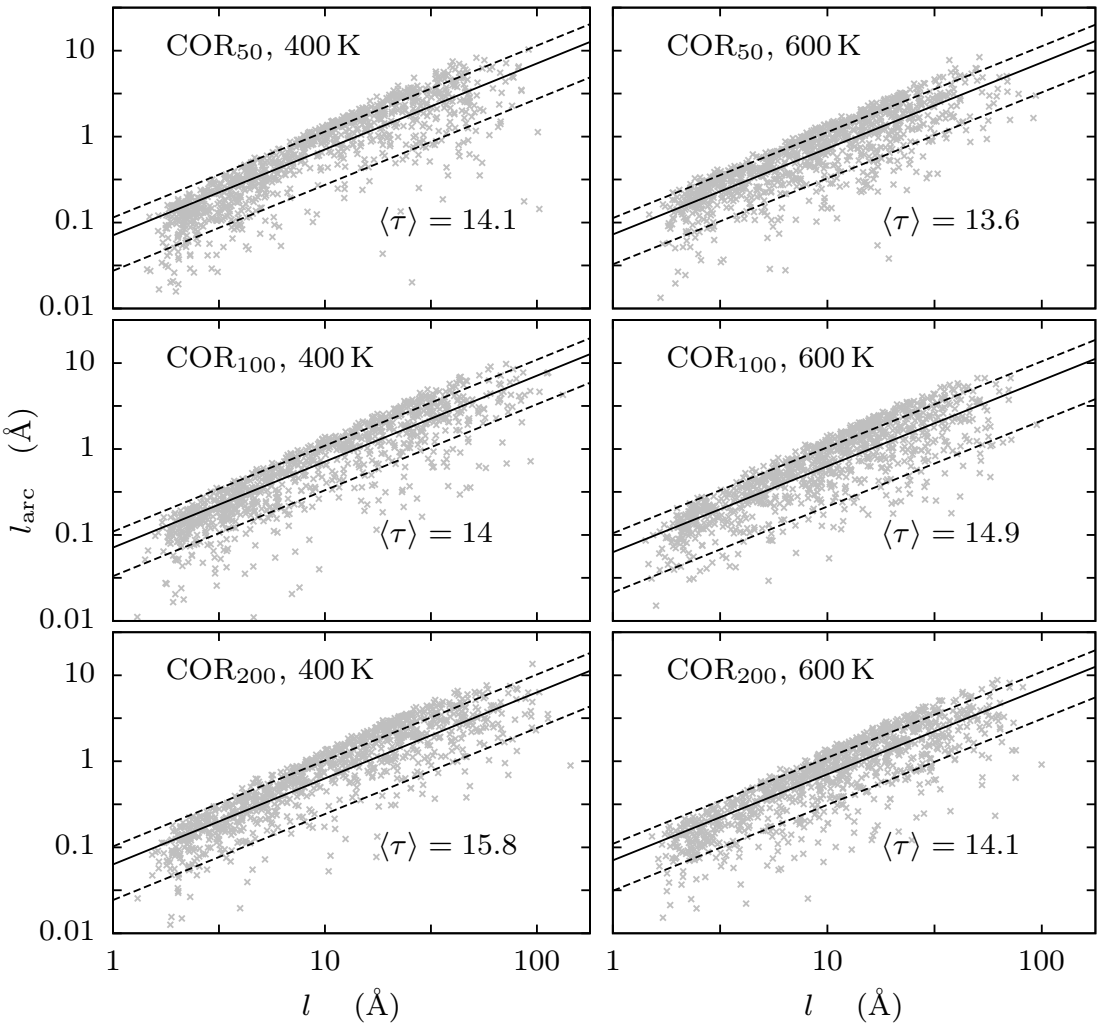

Figure 3: *Arc length versus actual path length. The solid black lines denote the linear regression of the l_{arc} versus l dependence with the slope corresponding to average tortuosity, $\langle\tau\rangle$. The black dashed lines denote the uncertainty bands.*

as described by Epstein [16] (i.e., $\langle\beta\rangle \approx \pi/2$). This suggests that the surface roughness may play a significant role in altering the shape of the actual nitrogen trajectory.

Table 1: *Average absorption-trapping-desorption angles.*

	$\langle\beta\rangle_{T=400\,\text{K}}$ (deg)	$\langle\beta\rangle_{T=600\,\text{K}}$ (deg)
$N = 50$	22.0 ± 0.8	20.4 ± 0.7
$N = 100$	19.0 ± 0.7	17.2 ± 0.6
$N = 200$	16.6 ± 0.6	14.5 ± 0.5

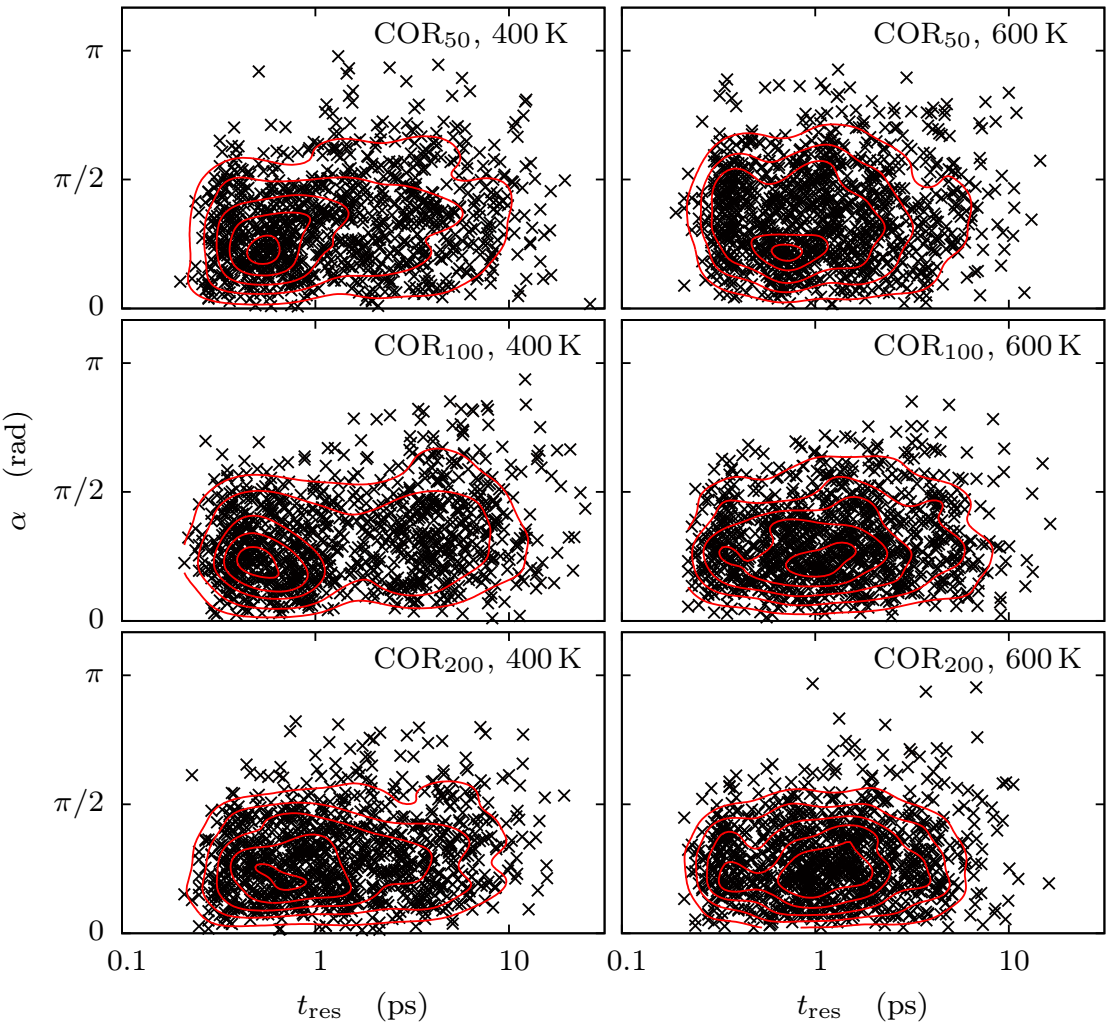

Figure 4: *Scattering angle versus residence time distributions. The solid red lines denote the contours of the 2-dimensional kernel density function estimate.*

Figure 6 shows the dependence of the actual path length on the residence time. It is important to note that the actual path length scales linearly with the observed residence time with a slope corresponding to the mean velocity of the nitrogen molecule during the residence period. The average standard deviation reveals that the velocity in most of the cases varies within the range of 36%. Further, a comparison with a so called "free regime", i.e., a regime in which the nitrogen molecule does not collide with any object reveals that the majority of the events exhibit velocity values that are not far from those expected when no collisions occur. This raises the question what role does the interaction energy play in the collisions? The trajectories of the nitrogen molecule are rather curved and at the same time the nitrogen molecule travels with a velocity that is in most of the cases similar to its thermal velocity without any collision taking place. The interaction energy must therefore affect mainly the shape of the trajectory.

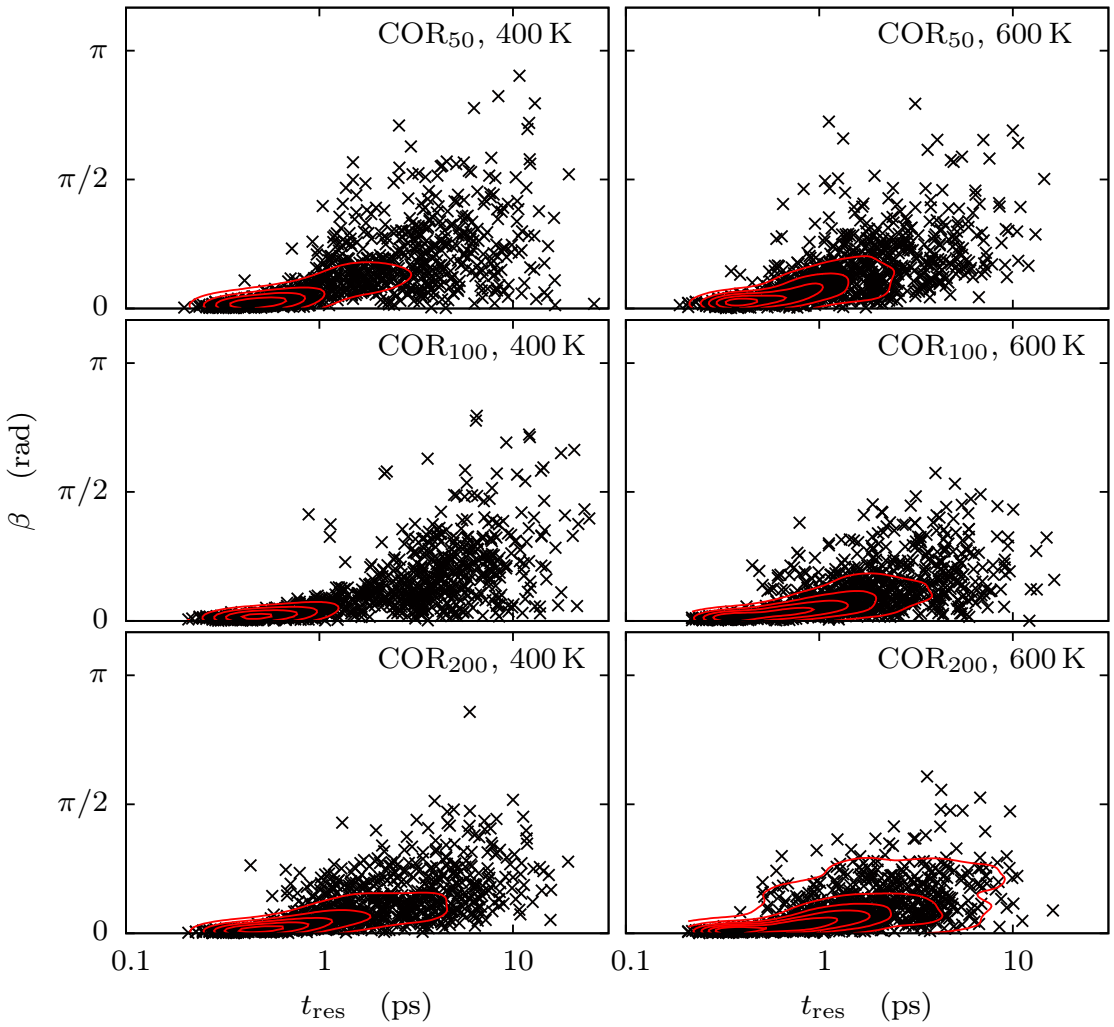

Figure 5: *Absorption-trapping-desorption angle versus residence time distributions. The solid red lines denote the contours of the 2-dimensional kernel density function estimate.*

Based on the recorded trajectories of the nitrogen probe that correspond to the longest residence times observed for COR_{100} clusters at 400K, we have identified four different interaction scenarios. These include: (i) pinning, (ii) trapping, (iii) H-jumps and (iv) the nitrogen probe buried inside the coronene cluster (cf. Figure 8). During its residence period, the nitrogen probe can appear in the proximity of two different local environments that can be characterised either as carbon- or hydrogen-rich, respectively. Based on the relative strength of the attractive forces between nitrogen and the remaining two atom types (carbon and hydrogen), the nitrogen probe can be either pinned to the coronene molecule carbons (pinning, cf. Figure 8.a and b) and its jumps become relatively short due to stronger attraction to carbon atoms or it can display relatively long jumps along the hydrogen rich edges of the coronene molecules (H-jumps, cf. Figure 8.d). A very

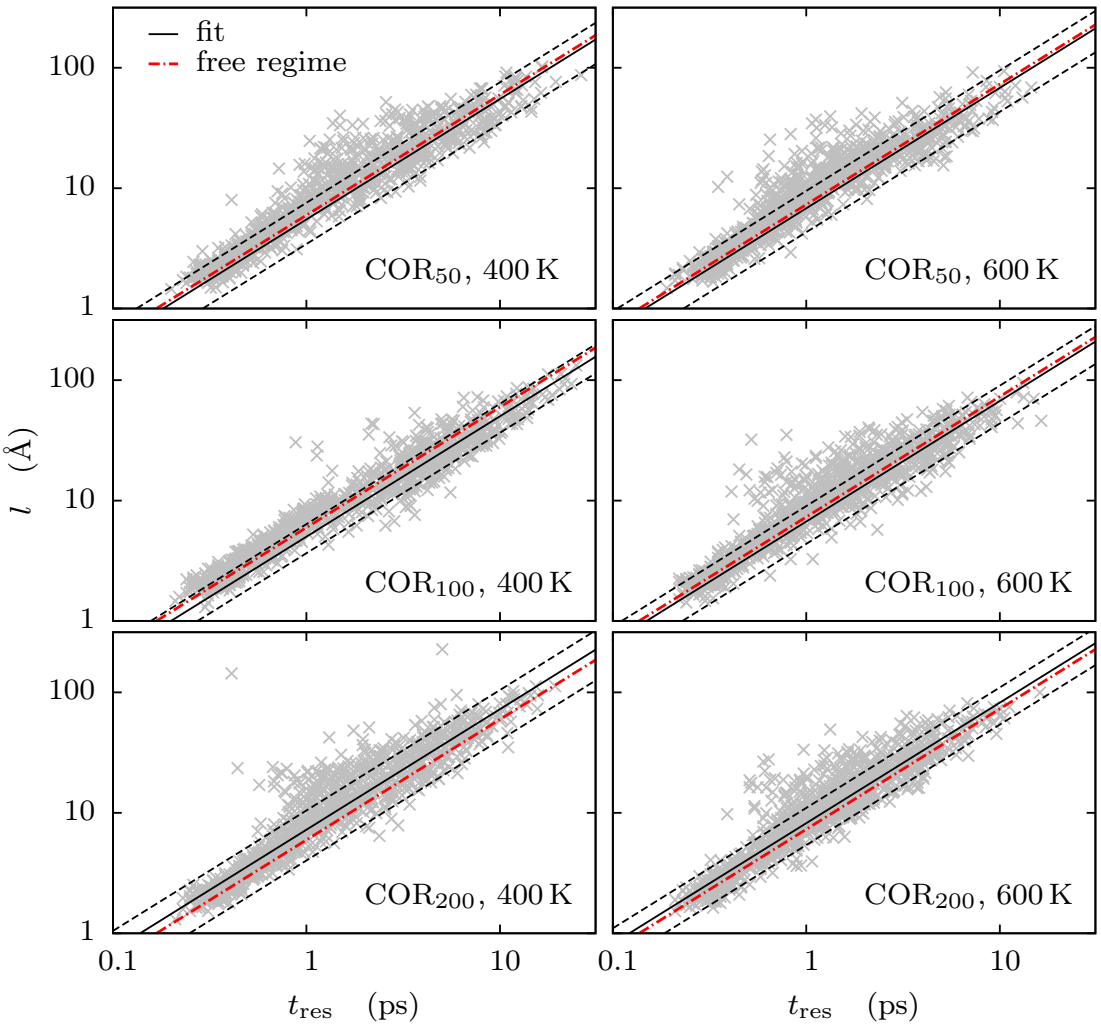

Figure 6: *Actual path length versus residence time. The solid black lines denote the linear regression of the l versus t_{res} dependence (fit) with the black dashed lines denoting the uncertainty bands. The dotted-dashed red lines corresponds to mean velocities of nitrogen molecule not colliding with anything (free regime).*

special situation can occur when the nitrogen probe appears in a surface cavity. In such case the nitrogen probe can become trapped due to increased number of interacting atoms (trapping, cf. Figure 8.c) or eventually even buried by another coronene molecule sliding at the clusters' surface (cf. Figure 8.e and f).

For practical reasons, it is crucial to understand what atoms belong to the most visited ones and whether the nitrogen molecule remains on the surface of the cluster or penetrates into its interior. In majority of the cases (cf. Figure 7) the nearest atoms to the nitrogen molecule are the hydrogen atoms, followed by the edge carbon atoms C_3. This finding becomes crucial when considering the feasibility of the generally accepted reaction mech-

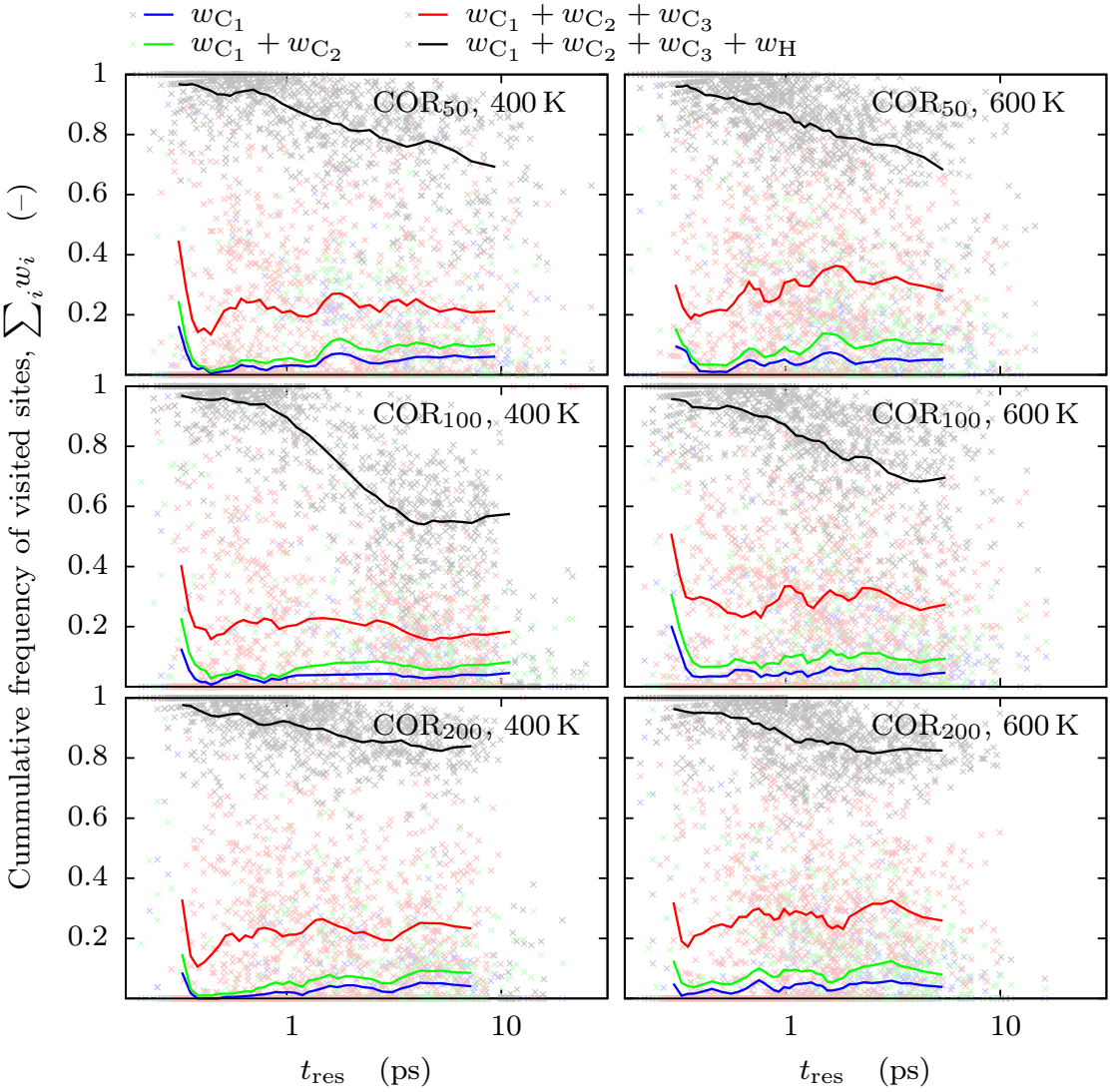

Figure 7: *Cummulative ratio of visited sites versus residence time. The trendlines correspond to moving averages of the data points.*

anisms (e.g., HACA, surface oxidation, hydrogen-abstraction-induced rearrangement or ring desorption processes, etc.) of chemical soot growth and inhibition [7, 18, 31, 32]. One reason hydrogen sites are seen more frequently visited by the nitrogen probe is due to the strong intermolecular bonding between the coronene π-bonds. The structure of the clusters can be described as turbostratic stacks of coronene molecules. For the clusters that are present in the solid state, the stacks are usually built of 8-10 coronene molecules and organised either in parallel or perpendicular fashion, as dictated by the character of the aromatic-aromatic interactions [19, 33]. This makes most of the carbon sites inaccessible to the nitrogen molecule which tends to move mainly in the proximity of the hydrogen atoms that are exposed to the surrounding area. Upon melting at 600K the increased thermal energy only allows the formation of smaller stacks, on average composed of 2-3 coronene molecules. Such situation is accompanied by an increase in the accessibility of

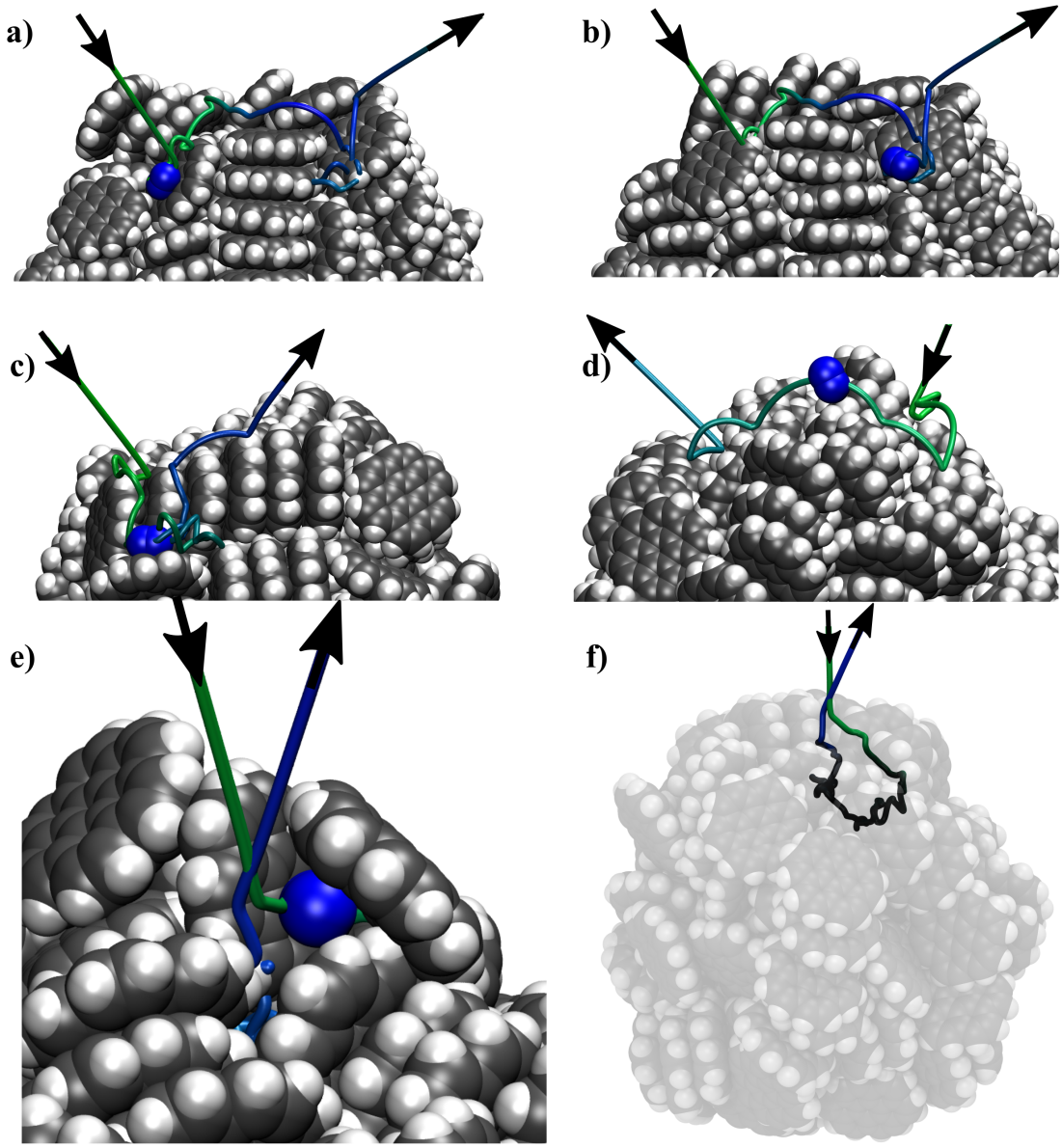

Figure 8: *Time evolution of nitrogen molecule interactions with the surface of a coronene cluster,* $N_{\mathrm{COR}} = 100$*. Three dimensional trajectories are shown as solid lines changing from green to blue with time. The molecular configuration are shown for different times along the trajectory at the time when the nitrogen is in the position shown. Four distinctly different types of trajectories can be observed, corresponding to pinning on the carbon rich face of the coronene (a, b), trapping in holes (c), H-jumps (d) and the nitrogen probe buried inside the coronene cluster (e, f).*

carbon sites compared with hydrogen due to the breakdown of the stacked structures and increased mobility of the coronene cluster constituent molecules.

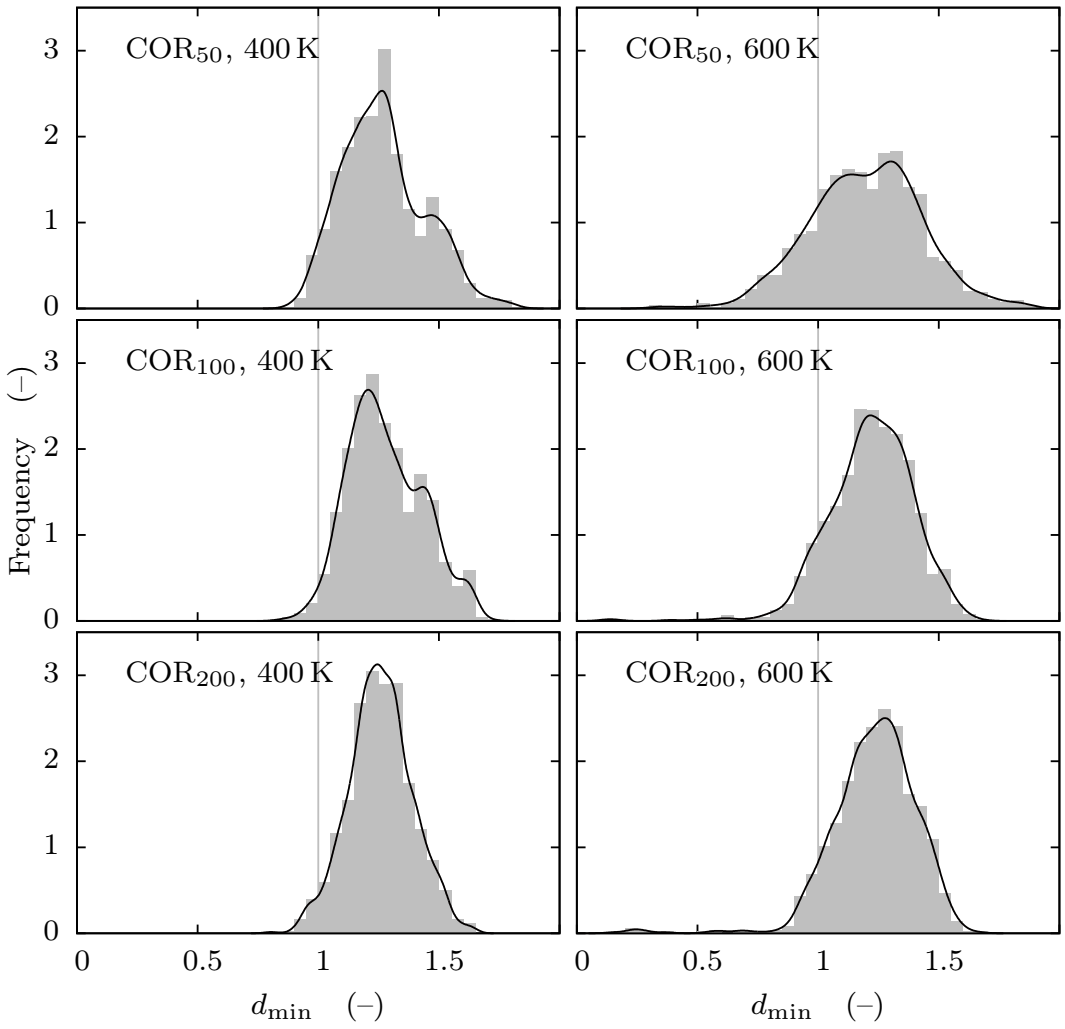

Figure 9: *Minimum nitrogen molecule-coronene cluster distance distributions. The minimum distance d_{min} is defined as the distance between the centres-of-mass of the nitrogen molecule and the coronene cluster normalised by the coronene cluster gyration radius.*

Figure 7 also shows that events that result in longer residence times can be characterised by increasing portion of jumps beyond the cut-off value. This fact does not mean that the nitrogen probe desorbs from the surface, as it still strongly interacts with the cluster (the pair potential energy minima are 0.346 nm for N-H interaction and 0.381 nm for N-C interaction, respectively).

Figure 9 shows the distributions of the minimum distance, d_{min}, between the center-of-mass of the nitrogen molecule and center-of-mass of the coronene cluster recorded during the surface residence period of the nitrogen molecule, normalised by the coronene cluster gyration radius. For the solid coronene clusters ($T = 400\,\text{K}$) the range of the recorded val-

ues suggests that the nitrogen molecule moves mainly on the clusters' surface ($d_{\min} \gtrsim 1$). On the other hand, in the case of liquid coronene clusters ($T = 600\,\mathrm{K}$) there is a slight chance of smaller $d_{\min}$ values (with the probability less than 5 events per 1000 simulations). Although the chance of nitrogen molecule entering the interior of the coronene cluster is very small, it is not completely impossible and is expected to increase with increasing temperature. Figure 8.e and f shows the trajectory of such an event. Due to the increased mobility of the coronene cluster constituent molecules the nitrogen can become buried underneath the surface layer molecules when the circumstances allow it (e.g., the presence of a nearby cavity). However, two factors may play an important role when interpreting the observed data: (i) the dependence of the mutual molecular distances inside the cluster on the radius of gyration, i.e., the minimum distance normalisation factor which tends to increase with decreasing density and (ii) the fact that high mobilities also cause increased mixing of the constituent molecules, i.e., molecules that have been present in the interior of the cluster may eventually reside at the clusters surface. Among other factors, such as a random migration of the nitrogen molecule towards areas characterised by strong interaction energy or transformation of the impact energy into internal rotational modes, the surface coverage events represent factors that can significantly prolong the residence time of the nitrogen molecule.

4 Conclusions

The residence time of the nitrogen molecule was shown to depend on the state of the coronene clusters (i.e., solid or liquid state), the local arrangements and the dynamics of the coronene molecules along the trapping trajectory. The relatively weak dependence of the residence time on the size of the clusters considered here suggests that for practical reasons it is not necessary to consider large polyaromatic hydrocarbon clusters to resemble all properties of such systems which may eventually lead to significant reductions in computational expenses.

Higher temperatures have the tendency to shorten the mean residence time, as the bimodality of the residence time distributions that results from a combination of specular and diffuse molecular scattering events, tends to disappear with increasing temperatures. The nitrogen molecule desorbs from the cluster in most of the observed cases before reaching on the opposite side of the cluster. As the recorded mean velocities of the nitrogen molecule suggest, the binding of the nitrogen molecule is relatively weak and the mutual interactions between the nitrogen molecule and the cluster affect mainly the shape of the nitrogen trapping trajectories by altering the direction. The diffusion paths are highly tortuous, on average an order of magnitude greater than the shortest distance between impact and desorption points. Three main gas-surface interaction dynamics were identified including pinning of the nitrogen molecule on the surface of coronene, jumping along hydrogen-rich faces and trapping in holes which at higher temperatures can lead to penetration of the molecule into the cluster. The drastic mixing of the coronene constituent molecules at high temperatures may cause the interior molecules to reach the surface layer and *vice versa* which can eventually alter the uniformity of the soot particle oxidation. If one accepts that coronene molecular clusters represent a physically reason-

able model of soot particles then the overall conclusion is that only molten particles can burn from the inside. However, the probability of soot-particle penetration by oxidation agents is statistically insignificant and surface oxidation will dominate.

Acknowledgments

This project was partly funded by the National Research Foundation (NRF), Prime Minister's Office, Singapore under its Campus for Research Excellence and Technological Enterprise (CREATE) programme.

A Appendix

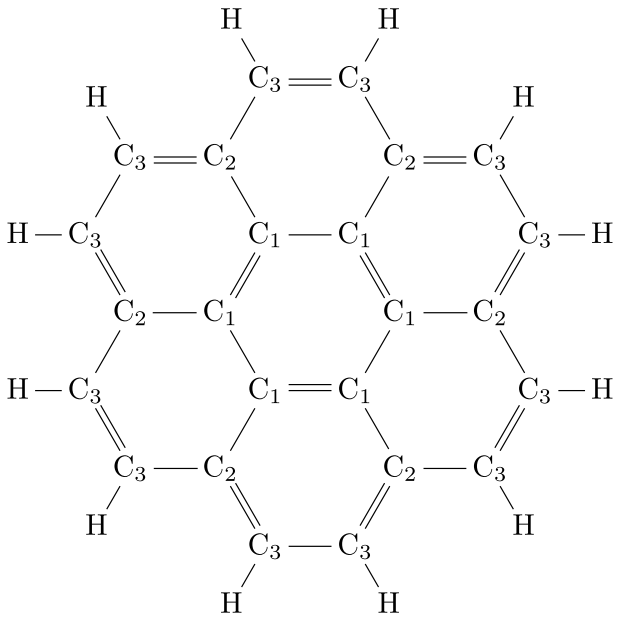

Figure 10: *Coronene molecule. Based on symetry, the coronene molecule composed of four types of atoms, i.e,* C_1*,* C_2*,* C_3 *and* H*, respectively.*

Table 2: *Intramolecular force field parameters*[†].

$u_{\text{bond}} = k_r(r-r_0)^2/2$		
	r_0 (nm)	k_r (kJ mol^{-1} nm^{-2})
C-C	0.14	392459.2
C-H	0.108	307105.6
N-N	0.1098	1382813.1
$u_{\text{ang}} = k_\varphi(\varphi-\varphi_0)^2/2$		
	φ_0 (deg)	k_φ (kJ mol^{-1} deg^{-2})
C-C-C	120	527.184
C-C-H	120	292.88
$u_{\text{dih}} = \sum_{k=0}^{5} c_k[\cos(\phi-\pi)]^k$		
$c_0 = 30.334\,\text{kJ mol}^{-1}$, $c_2 = -30.334\,\text{kJ mol}^{-1}$, $c_1 = c_3 = c_4 = c_5 = 0\,\text{kJ mol}^{-1}$		
$u_{\text{idih}} = k_\phi[1+\cos(n\phi-\phi_0)]$		
$k = 4.6024\,\text{kJ mol}^{-1}$, $n = 2$, $\phi_0 = \pi$		

[†]For more details, see the references [20, 21, 24].

Table 3: *isoPAHAP*[†] *force field parameters.*

$u_{vdw} = ge^{-\alpha(r-\rho)} - c_6 r^{-6}[1 - e^{-\beta r}\sum_{k=0}^{6}(\beta r)^k/k!]$

$\beta = 0.3115\,\text{nm}$, $g = 2.6253652\,\text{kJ mol}^{-1}$

	ρ (nm)	α (nm^{-1})	c_6 ($\text{kJ mol}^{-1}\,\text{nm}^6$)
C-C	0.3198	35.49	0.00174542
C-H	0.2623	33.18	0.000726727
H-H	0.218	26.54	0.000300841

[†]For more details, see the references [8, 43].

Table 4: *Williams 99*[†] *force field parameters.*

$u_{vdw} = ae^{-br} - cr^{-6}$

	a (kJ mol^{-1})	b (nm^{-1})	c ($\text{kJ mol}^{-1}\,\text{nm}^6$)
C-N	161397.7	35.4	0.001547677
H-N	34952.9	35.2	0.0006259595

[†]For more details, see the references [48, 49].

Table 5: *Generalised transferable electrostatic charges*[†].

$u_{el} = q_i q_j r_{ij}^{-1}$

	C_1	C_2	C_3	H	N
q (e)	−0.011022	0.18171	−0.239772	0.154428	–

[†]For more details, see the reference [42]. For numbering of the carbon atoms, see Figure 10.

References

[1] M. Alfè, B. Apicella, R. Barbella, J.-N. Rouzaud, A. Tregrossi, and A. Ciajolo. Structure-property relationship in nanostructures of young and mature soot in premixed flames. *Proceedings of the Combustion Institute*, 32(1):697–704, 2009. doi:10.1016/j.proci.2008.06.193.

[2] S. T. Aruna and A. S. Mukasyan. Combustion synthesis and nanomaterials. *Current Opinion in Solid State and Materials Science*, 12:44–50, 2008. doi:10.1016/j.cossms.2008.12.002.

[3] A. Bondi. Van der Waals volumes and radii. *Journal of Physical Chemistry*, 68(3): 441–451, 1964. doi:10.1021/j100785a001.

[4] M. L. Botero, E. M. Adkins, S. González-Calera, H. Miller, and M. Kraft. PAH structure analysis of soot in a non-premixed flame using high-resolution transmission electron microscopy and optical band gap analysis. *Combustion and Flame*, 164:250–258, 2016. doi:10.1016/j.combustflame.2015.11.022.

[5] M. L. Botero, D. Chen, S. González-Calera, D. Jefferson, and M. Kraft. HRTEM evaluation of soot particles produced by the non-premixed combustion of liquid fuels. *Carbon*, 96:459–473, 2016. doi:10.1016/j.carbon.2015.09.077.

[6] P. Buffat and J.-P. Borel. Size effect on the melting temperature of gold particles. *Physical Review A*, 13(6):2287–2298, 1976. doi:10.1103/PhysRevA.13.2287.

[7] M. S. Celnik, M. Sander, A. Raj, R. H. West, and M. Kraft. Modelling soot formation in a premixed flame using an aromatic-site soot model and an improved oxidation rate. *Proceedings of the Combustion Institute*, 32(1):639–646, 2009. doi:10.1016/j.proci.2008.06.062.

[8] D. Chen, T. S. Totton, J. W. J. Akroyd, S. Mosbach, and M. Kraft. Size-dependent melting of polycyclic aromatic hydrocarbon nano-clusters: A molecular dynamics study. *Carbon*, 67:79–91, 2014. doi:10.1016/j.carbon.2013.09.058.

[9] D. Chen, T. S. Totton, J. W. J. Akroyd, S. Mosbach, and M. Kraft. Phase change of polycyclic aromatic hydrocarbon clusters by mass addition. *Carbon*, 77:25–35, 2014. doi:10.1016/j.carbon.2014.04.089.

[10] D. Chen, J. Akroyd, S. Mosbach, and M. Kraft. Surface reactivity of polycyclic aromatic hydrocarbon clusters. *Proceedings of the Combustion Institute*, 35(2):1811–1818, 2015. doi:10.1016/j.proci.2014.06.140.

[11] D. Chen, J. W. J. Akroyd, S. Mosbach, D. Opalka, and M. Kraft. Solid-liquid transitions in homogenous ovalene, hexabenzocoronene and circumcoronene clusters: A molecular dynamics study. *Combustion and Flame*, 162(2):486–495, 2015. doi:10.1016/j.combustflame.2014.07.025.

[12] B. Coasne, A. Galarneau, F. Di Renzo, and R. J. M. Pellenq. Molecular simulation of nitrogen adsorption in nanoporous silica. *Langmuir*, 26(13):10872–10881, 2010. doi:10.1021/la100757b.

[13] R. A. Dobbins. Hydrocarbon nanoparticles formed in flames and diesel engines. *Aerosol Science and Technology*, 41(5):485–496, 2007. doi:10.1080/02786820701225820.

[14] R. A. Dobbins, R. A. Fletcher, and H.-C. Chang. The evolution of soot precursor particles in a diffusion flame. *Combustion and Flame*, 115(3):285–298, 1998. doi:10.1016/S0010-2180(98)00010-8.

[15] R. A. Dobbins, R. A. Fletcher, B. A. J. Benner, and S. Hoeft. Polycyclic aromatic hydrocarbons in flames, in diesel fuels, and in diesel emissions. *Combustion and Flame*, 144(4):773–781, 2006. doi:10.1016/j.combustflame.2005.09.008.

[16] P. S. Epstein. On the resistance experienced by spheres in their motion through gases. *Physical Review*, 23:710–733, 1924. doi:10.1103/PhysRev.23.710.

[17] M. Frenklach. Reaction mechanism of soot formation in flames. *Physical Chemistry Chemical Physics*, 4:2028–2037, 2002. doi:10.1039/b110045a.

[18] M. Frenklach and H. Wang. Detailed modeling of soot particle nucleation and growth. *Proceedings of the Combustion Institute*, 23:1559–1566, 1991.

[19] P. Grančič, R. Bylsma, H. Meekes, and H. M. Cuppen. Evaluation of all-atom force fields for anthracene crystal growth. *Crystal Growth & Design*, 15(4):1625–1633, 2015. doi:10.1021/cg5013507.

[20] K. P. Huber and G. Herzberg. *Molecular Spectra and Molecular Structure. IV. Constants of Diatomic Molecules*. Van Nostrand Reinhold Co., 1979.

[21] G. A. Kaminski, R. A. Friesner, J. Tirado-Rives, and W. L. Jorgensen. Evaluation and reparametrization of the OPLS-AA force field for proteins via comparison with accurate quantum chemical calculations on peptides. *Journal of Physical Chemistry B*, 105(28):6474–6487, 2001. doi:10.1021/jp003919d.

[22] Z. Li and H. Wang. Drag force, diffusion coefficient, and electric mobility of small particles. II. Application. *Physical Review E*, 68:061207, 2003. doi:10.1103/PhysRevE.68.061207.

[23] Z. Li and H. Wang. Gas-nanoparticle scattering: A molecular view of momentum accommodation function. *Physical Review Letters*, 95:014502, 2005. doi:10.1103/PhysRevLett.95.014502.

[24] G. Menconi and D. J. Tozer. Diatomic bond lengths and vibrational frequencies: Assessment of recently developed exchange-correlation functionals. *Chemical Physics Letters*, 360(1-2):38–46, 2002. doi:10.1016/S0009-2614(02)00787-X.

[25] P. Mitchell and M. Frenklach. Particle aggregation with simultaneous surface growth. *Physical Review E*, 67:061407, 2003. doi:10.1103/PhysRevE.67.061407.

[26] K. K. Nanda. Size-dependent melting of small particles: A classical approach. *European Journal of Physics*, 19(5):471, 1998.

[27] E. C. Neyts and A. Bogaerts. Numerical study of the size-dependent melting mechanisms of nickel nanoclusters. *The Journal of Physical Chemistry C*, 113(7):2771–2776, 2009. doi:10.1021/jp8058992.

[28] R. Niessner. The many faces of soot: Characterization of soot nanoparticles produced by engines. *Angewandte Chemie International Edition*, 53:12366–12379, 2014. doi:10.1002/anie.201402812.

[29] A. B. Palotás, L. C. Rainey, C. J. Feldermann, A. F. Sarofim, and J. B. Vander Sande. Soot morphology: An application of image analysis in high-resolution transmission electron microscopy. *Microscopy Research and Technique*, 33(3):266–278, 1996. doi:10.1002/(SICI)1097-0029(19960215)33:3<266::AID-JEMT4>3.0.CO;2-O.

[30] R. I. A. Patterson, J. Singh, M. Balthasar, M. Kraft, and W. Wagner. Extending stochastic soot simulation to higher pressures. *Combustion and Flame*, 145(3):638–642, 2006. doi:10.1016/j.combustflame.2006.02.005.

[31] A. Raj, M. Celnik, R. Shirley, M. Sander, R. Patterson, R. West, and M. Kraft. A statistical approach to develop a detailed soot growth model using PAH characteristics. *Combustion and Flame*, 156(4):896–913, 2009. doi:10.1016/j.combustflame.2009.01.005.

[32] A. Raj, P. L. W. Man, T. S. Totton, M. Sander, R. A. Shirley, and M. Kraft. New polycyclic aromatic hydrocarbon (PAH) surface processes to improve the model prediction of the composition of combustion-generated PAHs and soot. *Carbon*, 48(2):319–332, 2010. doi:10.1016/j.carbon.2009.09.030.

[33] M. Rapacioli, F. Calvo, F. Spiegelman, C. Joblin, and D. J. Wales. Stacked clusters of polycyclic aromatic hydrocarbon molecules. *The Journal of Physical Chemistry A*, 109(11):2487–2497, 2005. doi:10.1021/jp046745z.

[34] P. Roth. Particle synthesis in flames. *Proceedings of the Combustion Institute*, 31:1773–1788, 2007. doi:10.1016/j.proci.2006.08.118.

[35] M. Sander, R. I. A. Patterson, A. Braumann, A. Raj, and M. Kraft. Developing the PAH-PP soot particle model using process informatics and uncertainty propagation. *Proceedings of the Combustion Institute*, 33(1):675–683, 2011. doi:10.1016/j.proci.2010.06.156.

[36] C. A. Schuetz and M. Frenklach. Nucleation of soot: Molecular dynamics simulations of pyrene dimerization. *Proceedings of the Combustion Institute, Volume*, 29:2307–2314, 2002.

[37] J. Singh, M. Balthasar, M. Kraft, and W. Wagner. Stochastic modeling of soot particle size and age distributions in laminar premixed flames. *Proceedings of the Combustion Institute*, 30(1):1457–1465, 2005. doi:10.1016/j.proci.2004.08.120.

[38] R. I. Singh, A. M. Mebel, and M. Frenklach. Oxidation of graphene-edge six- and five-member rings by molecular oxygen. *The Journal of Physical Chemistry A*, 119: 7528–7547, 2015. doi:10.1021/acs.jpca.5b00868.

[39] S. E. Stein and A. Fahr. High-temperature stabilities of hydrocarbons. *The Journal of Physical Chemistry*, 89(17):3714–3725, 1985. doi:10.1021/j100263a027.

[40] R. Strobel and S. E. Pratsinis. Flame aerosol synthesis of smart nanostructured materials. *Journal of Materials Chemistry*, 17:4743–4756, 2007. doi:10.1039/b711652g.

[41] T. S. Totton, D. Chakrabarti, A. J. Misquitta, M. Sander, D. J. Wales, and M. Kraft. Modelling the internal structure of nascent soot particles. *Combustion and Flame*, 157:909–914, 2010. doi:10.1016/j.combustflame.2009.11.013.

[42] T. S. Totton, A. J. Misquitta, and M. Kraft. A transferable electrostatic model for intermolecular interactions between polycyclic aromatic hydrocarbons. *Chemical Physics Letters*, 510(1-3):154–160, 2011. doi:10.1016/j.cplett.2011.05.021.

[43] T. S. Totton, A. J. Misquitta, and M. Kraft. A quantitative study of the clustering of polycyclic aromatic hydrocarbons at high temperatures. *Physical Chemistry Chemical Physics*, 14:4081–4094, 2012. doi:10.1039/c2cp23008a.

[44] D. Van Der Spoel, E. Lindahl, B. Hess, G. Groenhof, A. E. Mark, and H. J. C. Berendsen. GROMACS: Fast, flexible, and free. *Journal of Computational Chemistry*, 26(16):1701–1718, 2005. doi:10.1002/jcc.20291.

[45] L. Verlet. Computer "experiments" on classical fluids. I. Thermodynamical properties of lennard-jones molecules. *Physical Review*, 159(1):98–103, 1967. doi:10.1103/PhysRev.159.98.

[46] A. Violi. Modeling of soot particle inception in aromatic and aliphatic premixed flames. *Combustion and Flame*, 139:279–287, 2004. doi:10.1016/j.combustflame.2004.08.013.

[47] H. Wang. Formation of nascent soot and other condensed-phase materials in flames. *Proceedings of the Combustion Institute*, 33:41–67, 2011. doi:10.1016/j.proci.2010.09.009.

[48] D. E. Williams. Improved intermolecular force field for crystalline hydrocarbons containing four- or three-coordinated carbon. *Journal of Molecular Structure*, 485-486:321–347, 1999. doi:10.1016/S0022-2860(99)00092-7.

[49] D. E. Williams. Improved intermolecular force field for molecules containing H, C, N, and O atoms, with application to nucleoside and peptide crystals. *Journal of Computational Chemistry*, 22(11):1154–1166, 2001. doi:10.1002/jcc.1074.